

Chaos based Berry phase detector

Cheng-Zhen Wang,¹ Chen-Di Han,¹ Hong-Ya Xu,¹ and Ying-Cheng Lai^{1,2,*}

¹*School of Electrical, Computer and Energy Engineering,
Arizona State University, Tempe, Arizona 85287, USA*

²*Department of Physics, Arizona State University, Tempe, Arizona 85287, USA*

(Dated: April 5, 2019)

The geometric or Berry phase, a characteristic of quasiparticles, is fundamental to the underlying quantum materials. The discoveries of new materials at a rapid pace nowadays call for efficient detection of the Berry phase. Utilizing α - T_3 lattice as a paradigm, we find that, in the Dirac electron optics regime, the semiclassical decay of the quasiparticles from a chaotic cavity can be effectively exploited for detecting the Berry phase. In particular, we demonstrate a one-to-one correspondence between the exponential decay rate and the geometric phase for the entire family of α - T_3 materials. This chaos based detection scheme represents an experimentally feasible way to assess the Berry phase and to distinguish the quasiparticles.

I. INTRODUCTION

The geometric phase, commonly referred to as the Pancharatnam-Berry phase or simply the Berry phase, is a fundamental characteristic of the quasiparticles of the underlying quantum material. When a system is subject to a cyclic adiabatic process, after the cycle is completed, the quantum state returns to its initial state except for a phase difference - the Berry phase¹⁻³. In general, the exact value of the Berry phase depends on the nature of the quasiparticles and hence the underlying material. For example, the Berry phases in monolayer graphene^{4,5} and graphite bilayers⁶ are $\pm\pi$ and 2π , respectively. In α - T_3 lattices, for different values of α , the Berry phases associated with the quasiparticles are distinct⁷.

Advances in physics, chemistry, materials science and engineering have led to the discoveries of new materials at an extremely rapid pace, e.g., the various two-dimensional Dirac materials⁸⁻¹⁰. These materials host a variety of quasiparticles with distinct physical characteristics including the Berry phase. To be able to detect Berry phase for a new material would generate insights into its physical properties for potential applications. Conventionally, this can be done using the principle of Aharonov-Bohm interference. For example, an atomic interferometer was realized in an optical lattice to directly measure the Berry flux in momentum space¹¹. Graphene resonators subject to an external magnetic field can be used to detect the Berry phase^{12,13}. Specifically, for a circular graphene p - n junction resonator, as a result of the emergence of the π Berry phase of the quasiparticles (Dirac fermions) when the strength of the magnetic field has reached a small critical value, a sudden and large increase in the energy associated with the angular-momentum states can be detected. In photonic crystals, a method was proposed to detect the pseudospin-1/2 Berry phase associated with the Dirac spectrum¹⁴. In such a system, the geometric Berry phase acquired upon rotation of the pseudospin is typically obscured by a large and unspecified dynamical phase. It was demonstrated¹⁴ that the analogy between a photonic crystal

and graphene can be exploited to eliminate the dynamical phase, where a minimum in the transmission arises as a direct consequence of the Berry phase shift of π acquired by a complete rotation of the pseudospin about a perpendicular axis.

In this paper, we report a striking phenomenon in 2D Dirac materials, which leads to the principle of chaos based detection of Berry phase. To be concrete, we consider the entire α - T_3 material family. An α - T_3 material can be synthesized by altering the honeycomb lattice of graphene to include an additional atom at the center of each hexagon which, for $\alpha = 1$, leads to a T_3 or a dice lattice that hosts pseudospin-1 quasiparticles with a conical intersection of triple degeneracy in the underlying energy band¹⁵⁻⁴¹. An α - T_3 lattice is essentially an interpolation between the honeycomb lattice of graphene and a dice lattice, where the normalized coupling strength α between the hexagon and the central site varies between zero and one^{7,42-46}, as shown in Fig. 1(a). Theoretically, pseudospin-1 quasiparticles are described by the Dirac-Weyl equation^{16,17,34}. Suppose we apply an appropriate gate voltage to generate an external electrostatic potential confinement or cavity of α - T_3 lattice. The mechanism for Berry phase detection arises in the short wavelength or semiclassical regime, where the classical dynamics are relevant and can be treated according to ray optics with reflection and transmission laws determined by Klein tunneling - the theme of the emergent field of Dirac electron optics (DEO)^{13,47-75}. If the shape of the cavity is highly symmetric, e.g., a circle, the classical dynamics of the quasiparticles are integrable. However, if the cavity boundaries are deformed from the integrable shape, chaos can arise. We focus on the energy regime $V_0/2 < E < V_0$ in which Klein tunneling is enabled, where V_0 is the height of the potential [Fig. 1(b)], so that the relative effective refractive index n inside the cavity falls in the range $[-\infty, -1]$. As a result, there exists a critical angle for total internal reflections. For different values of the material parameter α , the physical characteristics of the quasiparticles, in particular the values of the Berry phase, are different. Our central idea is then that, for a fixed cavity shape, the semiclassical

decay laws for quasiparticles corresponding to different values of α would be distinct. If the classical cavity dynamics contain a regular component, the decay laws will be algebraic^{76–80}, but we find that the differences among them will not be statistically significant enough to allow lattices of different values of α to be distinguished. However, when the cavity is deformed so that the classical dynamics are fully chaotic, the decay law becomes exponential⁸¹. The striking phenomenon is that the exponential decay rate for different values of α can be statistically distinguished to allow the Berry phase of the quasiparticles to be unequivocally detected, leading to the birth of chaos based Berry phase detectors. We note that in microcavity optics, classical chaos can be exploited to generate lasing with a high quality factor and good emission directionality at the same time^{82–92}.

II. HAMILTONIAN AND DIRAC ELECTRON OPTICS

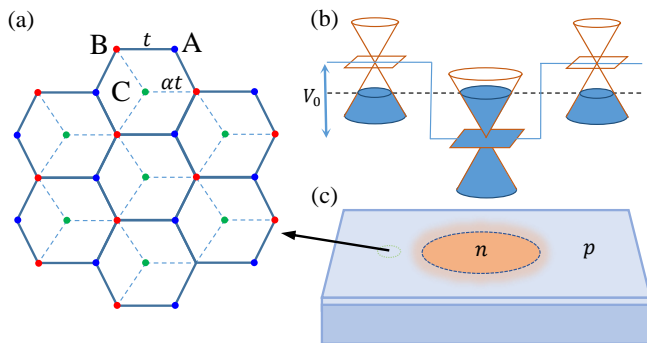


FIG. 1. Schematic illustration of an α -T₃ cavity and the energy dispersion relation. (a) α -T₃ lattice structure. (b) The electron and hole energy dispersion relations in different spatial regions. (c) A possible scheme of experimental realization of the cavity through an applied gate voltage. The amount of the voltage is such that the quasiparticles are in the Klein-tunneling regime.

The α -T₃ lattice system has the advantage of generating a continuous spectrum of quasiparticles with systematically varying Berry phase through the tuning of the value of the parameter α in the unit interval. At the two opposite ends of the spectrum, i.e., $\alpha = 0, 1$, the quasiparticles are pseudospin-1/2 Dirac fermions and pseudospin-1 Dirac-Weyl particles, respectively. As illustrated in Fig. 1, the lattice has three nonequivalent atoms in one unit cell, and the interaction strength is t between A and B atoms and αt between B and C atoms, where t is the nearest neighbor hopping energy of the graphene lattice. A cavity of arbitrary shape can be realized by applying an appropriate gate voltage through the STM technique^{13,60,93}, as shown in Fig. 1(c). We consider circular and stadium shaped cavities that exhibit integrable and chaotic dynamics, respectively, in the classi-

cal limit⁹⁴. The low-energy Hamiltonian for the α -T₃ system about a K point in the hexagonal Brillouin zone is^{42,45} $\hat{H} = \hat{H}_{kin} + V(x)\hat{I}$, where \hat{H}_{kin} is the kinetic energy, $V(x)$ is the applied potential that forms the cavity, and I is the 3×3 identity matrix. The coupling strength α can be conveniently parameterized as $\alpha = \tan \psi$. The kinetic part of the rescaled Hamiltonian (by $\cos \psi$) is

$$\hat{H}_{kin} = \begin{bmatrix} 0 & f_k \cos \psi & 0 \\ f_k^* \cos \psi & 0 & f_k \sin \psi \\ 0 & f_k^* \sin \psi & 0 \end{bmatrix}, \quad (1)$$

where $f_k = v_F(\xi k_x - i k_y)$, v_F is the Fermi velocity, $\mathbf{k} = (k_x, k_y)$ is the wave vector, and $\xi = \pm$ is the valley quantum number associated with K and K' , respectively. In the semiclassical regime where the particle wavelength is much smaller than the size of the cavity so that the classical dynamics are directly relevant, the DEO paradigm can be instated to treat the particle escape problem, which is analogous to decay of light rays from a dielectric cavity. In DEO, the essential quantity is the transmission coefficient of a particle through a potential step, which can be obtained by wavefunction matching as⁴⁵

$$T = \frac{4ss' \cos \theta \cos \phi}{2 + 2ss' \cos(\theta + \phi) - \sin^2 2\psi (s \sin \theta - s' \sin \phi)^2}, \quad (2)$$

where $s = \pm$ and $s' = \pm$ with the plus and minus signs denoting the conduction and valence band, respectively, and incident and transmitted angles are ϕ and θ , respectively. Imposing conservation of the component of the momentum tangent to the interface, we get

$$\sin \theta = (E/|E - V_0|) \sin \phi.$$

(More details about electron transmission through a potential step can be found in Appendix A). Our focus is on the survival probability of the quasiparticles from an α -T₃ cavity for the entire material spectrum: $0 \leq \alpha \leq 1$.

We set the amount of the applied voltage such that the energy range of the quasiparticles is $V_0/2 < E < V_0$ (the Klein tunneling regime). In the optical analog, the corresponding relative effective refractive index inside the cavity is $n = E/(E - V_0)$ and that outside of the cavity is $n = 1$. Due to Klein tunneling, the range of relative refractive index in the cavity is negative: $-\infty < n < -1$. As a result, a critical angle exists for the tunneling of electrons through a simple static electrical potential step, which is $\sin \phi_c = (V_0 - E)/E$ and is independent of the α value⁴⁵. This behavior is exemplified in the polar representation of the transmission in Fig. 2(a), which shows that the value of the transmission increases with α . As the value of α is varied in the unit interval, the critical angle remains unchanged.

III. RESULTS

1. Algebraic decay of α - T_3 quasiparticles from a circular (integrable) cavity

The classical phase space contains Kolmogorov-Arnold-Moser (KAM) tori and an open area through which particles (rays) escape. Initializing an ensemble of particles (e.g., 10^7) in the open area, the survival probability time distribution (SPTD) is given by

$$P_{sv}(t) = \int_0^L ds \int_{-p_c}^{p_c} dp I(s, p) R(p)^{N(t)}, \quad (3)$$

where L is the boundary length, $p_c = \sin \phi_c = 1/|n|$ with ϕ_c being the critical angle for total internal reflection, $R(p) = 1 - T$ is the reflection coefficient for the α - T_3 quasiparticles with transmission T defined in Eq. (2), $N(t) = t/(2 \cos \phi)$ is the number of bounces off the boundary, and $I(s, p) = |n|/2L$ is the uniform initial distribution.

Consider a circle of unit radius. Using the length of the ray trajectory as the time scale, we can rewrite Eq. (3) as

$$P_{sv}(t) = |n| \int_0^{\phi_c} d\phi \cos \phi \exp \left[-\frac{t}{2 \cos \phi} \ln \left(\frac{1}{R} \right) \right], \quad (4)$$

with

$$R^{-1} = 1 + \frac{-4 \cos \theta \cos \phi}{2 + 2 \cos(\theta - \phi) - \sin^2 2\psi (\sin \theta + \sin \phi)^2}. \quad (5)$$

The behavior of the particle transmission coefficient shown in Fig. 2(a) indicates that particles near the critical angle ϕ_c can survive for a longer period of time in the cavity. We can then expand the $\ln(\frac{1}{R})$ term about the critical angle ϕ_c by defining a new variable χ with $\phi = \phi_c - \chi$ and exploiting the approximation $\chi \rightarrow 0$. We have

$$\ln \left(\frac{1}{R} \right) \approx \frac{4\sqrt{2|n|} \cos \phi_c \cos \phi_c}{2 + [2|n| - \sin^2 2\psi (|n| + 1)^2 \sin^2 \phi_c]} \cdot \chi^{1/2}. \quad (6)$$

Substituting Eq. (6) into Eq. (4), we obtain the SPTD as

$$\begin{aligned} P_{sv} &= \frac{1}{4} t^{-2} \{ 2 + [2|n| - \sin^2 2\psi (|n| + 1)^2] \frac{1}{|n|^2} \}^2 \\ &= C(n, \psi) t^{-2} \end{aligned} \quad (7)$$

This indicates that the quasiparticles decay algebraically from the cavity and the value of the decay exponent is two, regardless of the value of α . For certain value of $|n|$, as the value of α changes from zero to one, the decay coefficient $C(n, \psi)$ decreases, as shown in Fig. 2(b). Here, SPTD for the circular cavity is calculated with 10^7

random initial points in the open region of the phase space. The trajectory from each point is traced with the reflection coefficient $R(p)$ at boundary. The survival probability between t and $t + \Delta$ with $\Delta = 1$ is calculated with the initial probability one at $t = 0$. From Fig. 2(b), we see that both theoretical and numerical results show an algebraic behavior in the long time regime with the exponent of two.

Experimentally, to distinguish the nature of the quasiparticles and to detect the Berry phase, the decay coefficient is not a desired quantity to measure as it reflects the short time behavior of the decay process. In fact, it not only depends the nature of the material (as determined by the value of α) but also on the detailed system design. The long time behavior of the decay is characterized by the algebraic decay exponent, which does not depend on the details of the experimental design and, hence, it can possibly be exploited for Berry phase detection. However, for an integrable cavity, the algebraic decay exponent remains constant as the value of α is changed, as shown in Fig. 2(b). It is thus not feasible to distinguish the quasiparticles by their long time behavior, ruling out integrable cavities as a potential candidate for detecting the Berry phase.

2. Exponential decay of α - T_3 quasiparticles from a chaotic cavity

For the stadium cavity, the classical dynamics are chaotic, leading to random changes in the direction of the propagating ray. In this case, the survival probability of the quasiparticles in the cavity decays exponentially with time, as shown in Fig. 2(c), where the long time behavior is determined by the exponential decay rate. The striking phenomenon is that the decay rate increases monotonically as the value of the material parameter α is increased from zero to one, suggesting the possibility of using the exponential decay rate to distinguish the α - T_3 materials and to detect the intrinsic Berry phase. The difference in the decay rate can be further demonstrated by calculating its dependence on the absolute value $|n|$ for different values of α , as shown in Fig. 3(a). For small values of $|n|$, the difference in the decay rate is relatively large, indicating a stronger ability to discern the α - T_3 quasiparticles. For large values of $|n|$, the difference in the decay rate is somewhat reduced. This is expected because, as the value of $|n|$ is increased from one, the transmission for the materials at the two ends of the α - T_3 spectrum, namely graphene and pseudospin-1 lattice, decreases continuously. For $|n| \rightarrow \infty$, the transmission tends to zero. This result indicates that, the optimal regime to discern the quasiparticles for α - T_3 occurs for $|n|$ above one but not much larger, corresponding to the regime where the particle energy is slightly above half of the potential height.

In general, for a given value of α , the exponential decay rate is inversely proportional to n , which can be ar-

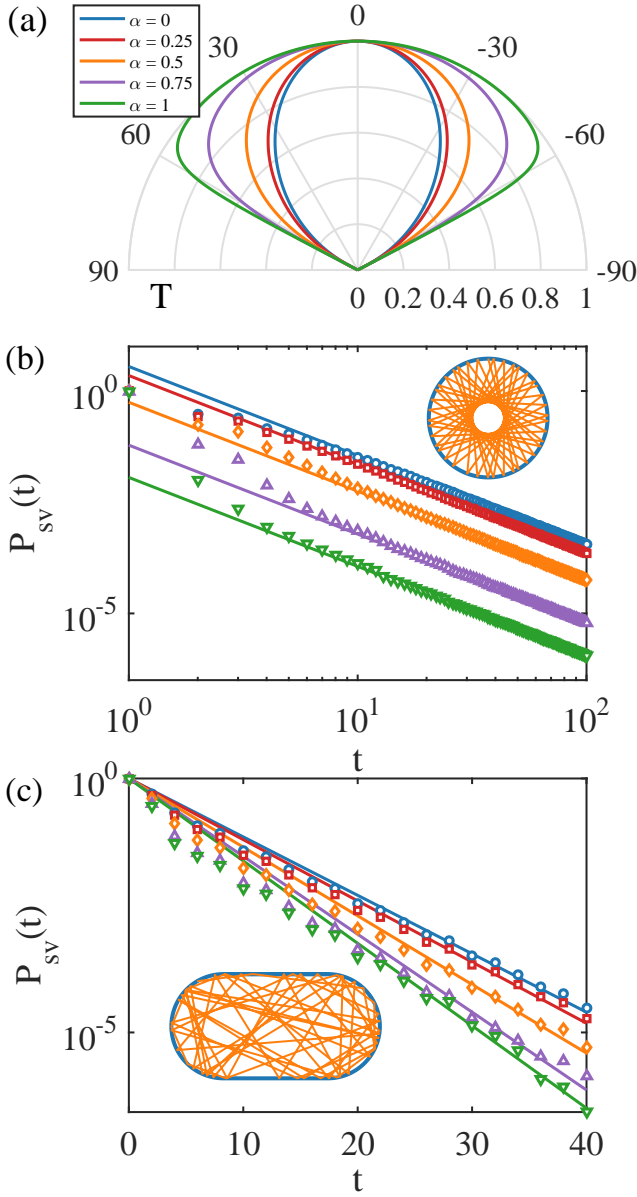


FIG. 2. Semiclassical decay of quasiparticles from a cavity in an α - T_3 lattice. For particle energy $E = 0.53V_0$ (within Klein tunneling regime) and relative refractive index $n = -1.1277$ inside of the cavity, (a) transmission T across a potential step as a function of incident angle ϕ for a number of equally spaced α values. (b) SPTD for the circular (integrable) cavity on a double logarithmic plot, where the blue circles, red squares, orange diamonds, purple up-triangles, and green down-triangles are numerical results for the five α values in (a), respectively, and the solid lines are the theoretical predictions. The decay is algebraic but the decay exponent is a constant independent of the value of α . (c) SPTD for a stadium shaped (chaotic) cavity of semicircle radius one and straight edge of length two on a semi-logarithmic plot. The color legends are the same as in (b). In this case, the decay is exponential and its rate depends on the value of α . Measuring the exponential decay rate then gives the value of α and the corresponding Berry phase of the underlying material lattice system.

gued, as follows^{95,96}. For $P_{sv}(t) \sim \exp(-\gamma t)$, we have $dP_{sv}(t)/dt \sim -\gamma \cdot P_{sv}(t) \sim -(\langle T(p) \rangle / \langle d \rangle) \cdot P_{sv}(t)$, where $\langle T(p) \rangle$ and $\langle d \rangle$ are the average transmission and the distance between two consecutive collisions in the chaotic cavity. The decay rate can then be obtained in terms of the steady probability distribution $P_s(s, p)$ as:

$$\gamma = \langle T(p) \rangle / \langle d \rangle = \langle d \rangle^{-1} \int_0^L ds \int_{-1}^1 dp P_s(s, p) T(p) \quad (8)$$

In the Klein tunneling regime $V_0/2 < E < V_0$ ($-\infty < n < -1$), we can derive an analytical expression for the exponential decay rate based on a simple model of the steady probability distribution (SPD) for the stadium-shaped cavity that generates fully developed chaos in the classical limit⁹⁵. Specifically, we assume that the SPD is a uniform distribution over the whole phase space except the open regions related to the linear segments of the stadium boundary. The decay rate can then be expressed in terms of the steady probability distribution:

$$\gamma = \frac{2\pi R}{2(\pi A/L)(L - 2l/|n|)} \int_{-1/|n|}^{1/|n|} dp T(p), \quad (9)$$

where $T(p)$ is the transmission coefficient defined in Eq. (2), the average path length of ray trajectory segments between two successive bounces is $\langle d \rangle = \pi A/L$, with $A = \pi R^2 + 2Rl$ and $L = 2\pi R + 2l$ being the area and boundary length of the stadium, respectively. Substituting the expressions $\sin \theta = |n|p$, $\cos \theta = -\sqrt{1 - \sin^2 \theta} = -\sqrt{1 - n^2 p^2}$, $\sin \phi = p$, and $\cos \phi = \sqrt{1 - p^2}$ into the expression of $T(p)$, we get

$$T = 4\sqrt{1 - p^2} \sqrt{1 - n^2 p^2} / [2 + 2\sqrt{1 - p^2} \sqrt{1 - n^2 p^2} + 2|n|p^2 - \sin^2 2\psi(n^2 p^2 + p^2 + 2|n|p^2)]. \quad (10)$$

In the limit $|n| \approx 1$, imposing change of variable $x = n^2 p^2$ to get $dp = dx / (2|n|\sqrt{x})$, we can write the decay rate in terms of variable x as

$$\begin{aligned} \gamma &= \frac{2\pi R}{2(\pi A/L)(L - 2l/|n|)} \int_0^1 \frac{dx}{\sqrt{x}} T(x) \\ &= \frac{2\pi R}{2(\pi A/L)(L - 2l/|n|)} \int_0^1 \frac{dx}{\sqrt{x}} (1 - x)(1 - \sin^2 2\psi \cdot x)^{-1} \\ &= \frac{2\pi R}{2(\pi A/L)(L - 2l/|n|)} B(1/2, 2) F(1, 1/2; 5/2; \sin^2 2\psi) \\ &\approx \frac{2\pi R}{2(\pi A/L)(L - 2l/|n|)} \frac{4}{3} \cdot (1 + \frac{1}{5} \sin^2 2\psi + \dots), \quad (11) \end{aligned}$$

where $B(x, y) = \Gamma(x)\Gamma(y)/\Gamma(x + y)$ is the beta function and $F(\alpha, \beta; \gamma; z)$ is the Gauss hypergeometric function.

In the $|n| \gg 1$ regime, we use the change of variable $x = np$ to simplify the decay rate integral. The decay rate becomes

$$\gamma = \frac{4\pi R}{2(\pi A/L)L|n|} \int_0^1 \frac{4\sqrt{1 - x^2}}{2 + 2\sqrt{1 - x^2} - \sin^2(2\psi)x^2}, \quad (12)$$

which is inversely proportional to the absolute value of the refractive index $|n|$. More importantly, the decay rate depends on the material parameter α monotonically ($\alpha = \tan \psi$, with α increasing from zero to one). We note that, the theoretical results in Fig. 2(c) is obtained by doing the integration formula (9) directly. The approximation used to derive E qs. (11) and (12) is to facilitate an analytic demonstration of the scaling of the decay rate with n . The formulas also reveal that the decay rate increases monotonically with α .

Numerically, we choose the stadium shape with the semicircle radius to be one and the length of the straight long edge to be two. In the calculation, we use a random ensemble of 10^7 initial points spread over the whole phase space and trace the survival probability with time, which is scaled by the length of trajectory as in the case of a circular cavity. The numerical results are consistent with the theoretical cases based on SPD approximation, as shown in Fig. 2(c).

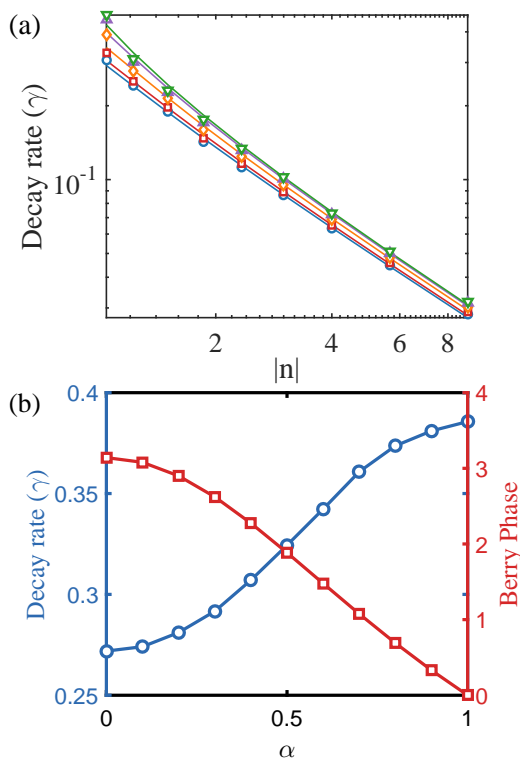


FIG. 3. Dependence of the semiclassical exponential decay rate from a chaotic cavity on the effective refractive index and the detection of the Berry phase. (a) For $\alpha = 0, 0.25, 0.5, 0.75, 1$, the decay rate versus the refractive index, where the blue circles, red squares, orange diamonds, purple up-triangles and green down-triangles are the respective numerical results and the dashed curves are theoretical predictions. (b) For $E/V_0 = 0.53$, detection of Berry phase (red squares) based on the decay rate (blue circles). As the value of α is changed from zero to one, there is a one-to-one correspondence between the exponential decay rate and the Berry phase.

3. Detection of Berry phase

The Berry phase associated with an orbit in the conical bands is given by⁷

$$\phi_{\xi}^B = \pi \xi \cos(2\psi) = \pi \xi \left(\frac{1 - \alpha^2}{1 + \alpha^2} \right). \quad (13)$$

For the flat band, the Berry phase is

$$\phi_{0,\xi}^B = -2\pi \xi \cos(2\psi) = -2\pi \xi \left(\frac{1 - \alpha^2}{1 + \alpha^2} \right). \quad (14)$$

We take $\xi = \pm 1$ for the K and K' valleys, respectively. For $\xi = 1$, the dependence of the Berry phase on α is shown in Fig. 3(b). As the value of α is increased from zero to one, the Berry phase decreases monotonically from π to zero. At the same time, the exponential decay rate increases monotonically. There is then a one-to-one correspondence between the decay rate and the Berry phase for the entire spectrum of α -T₃ materials, justifying a semiclassical chaotic cavity as an effective Berry phase detector.

IV. DISCUSSION

To summarize, we uncover a phenomenon in relativistic quantum chaos that can be exploited to detect the Berry phase of two-dimensional Dirac materials. In particular, for the spectrum of α -T₃ materials, in the semiclassical regime, the decay of the quasiparticles from a chaotic cavity depends on the intrinsic material parameter. Experimentally, the cavity can be realized through a gate voltage, where locally the boundary of the cavity is effectively a potential step. When the Fermi energy of the quasiparticles is above half but below the potential height, the system is in the Klein tunneling regime, rendering applicable Dirac electron optics. In this case, the relative effective refractive index inside the cavity is between negative infinity and minus one, so a critical angle exists for the semiclassical ray dynamics. Because of the close interplay between Klein tunneling and the value of the Berry phase, measuring the quasiparticle escape rate leads to direct information about the Berry phase and for differentiating the α -T₃ materials. Our analysis and calculation have validated this idea - we have indeed found a one-to-one correspondence between the exponential decay rate and the value of the Berry phase. In terms of basic physics, our finding builds up a connection, for the first time, between classical chaos and Berry phase. From an applied standpoint, because of the fundamental importance of Berry phase in determining the quantum behaviors and properties of materials, our work, relative simplicity notwithstanding, provides an effective and experimentally feasible way to assess the Berry phase for accurate characterization of the underlying material. This may find broad applications in materials science and engineering where new nanomaterials are being discovered

at a rapid pace, demanding effective techniques of characterization.

A possible experimental scheme to detect the Berry phase for the family of α -T₃ materials is as follows. For each type of material, one first makes a chaotic cavity (e.g., a stadium or a heart shaped domain). One then measures the quasiparticle decay rate for the graphene cavity (corresponding to $\alpha = 0$). Since the Berry phase of graphene is known, one can use the measurement as a baseline for calibrating the results from other materials in the family. Finally, making use of the one-to-one correspondence between the curves of the decay rate and the Berry phase versus the material parameter α as theorized in this paper, one can detect the actual Berry phase for the material with any value of α for $0 < \alpha \leq 1$.

ACKNOWLEDGMENT

We would like to acknowledge support from the Vannevar Bush Faculty Fellowship program sponsored by the Basic Research Office of the Assistant Secretary of Defense for Research and Engineering and funded by the Office of Naval Research through Grant No. N00014-16-1-2828.

Appendix A: Band structure and wavevectors across a potential step

To better understand the optical-like decay behavior of quasiparticles from a cavity formed by an electrostatic gate potential, we illustrate the electron band structure and the wavevectors across a potential step associated with a transmission process, as shown in Fig. 4. We also indicate a classification scheme of the regimes with different values of the refractive index, which are determined by different values of the applied potential relative to the Fermi energy. In particular, there are regimes of positive and negative values of the refractive index with respect to cases where a critical angle exists or is absent. For convenience, the incident electron is assumed to be in the conduction band, i.e., with a positive Fermi energy, and we vary the potential height V_0 . When V_0 is larger than the Fermi energy, the transmitted electron is in the valence band. In this case, the wavevector has a negative x and a positive y component but the direction of the velocity remains unchanged, leading to a negative value of the refractive index.

More specifically, for gate potential height in the range $V_0/2 < E < V_0$, the value of the refractive index $n = E/(E - V_0)$ falls in the range $-\infty < n < -1$. There is a critical angle in this case, which is determined by $\sin \theta = 1 = (E/|E - V_0|) \sin \phi_c$. The transmission angle

can be obtained in terms of incident angle ϕ as

$$\begin{aligned} \theta &= \pi - \tan^{-1} \frac{\sin \phi \cdot E/V_0}{\sqrt{(1 - E/V_0)^2 - (\sin \phi \cdot E/V_0)^2}} \\ &= \pi + \tan^{-1} \frac{n \sin \phi}{\sqrt{1 - (n \sin \phi)^2}}. \end{aligned} \quad (\text{A1})$$

where the relations $\sin \theta = (E/|E - V_0|) \sin \phi$ and $\cos \theta = -\sqrt{1 - \sin^2 \theta}$ have been used. The band structure and angles corresponding to the wavevectors are shown in Figs. 4(a,e), respectively.

In the regime where the potential height satisfies $0 < E < V_0/2$, the value of the refractive index is in the range $-1 < n < 0$. As a result, there is no critical angle. The transmission angle can be obtained in the same form as Eq. (A1). A schematic illustration of the band structure and the wavevector angles for this case are shown in Figs. 4(b,f), respectively.

For $V_0 < 0 < E$, the value of the refractive index is in the positive range $0 < n < 1$, because both the incident and transmitted electron is in the conduction band. There is no critical angle in this case. The transmission angle can be obtained as

$$\begin{aligned} \theta &= \tan^{-1} \frac{\sin \phi \cdot E/V_0}{\sqrt{(1 - E/V_0)^2 - (\sin \phi \cdot E/V_0)^2}} \\ &= \tan^{-1} \frac{n \sin \phi}{1 - (n \sin \phi)^2}. \end{aligned} \quad (\text{A2})$$

where the relations $\sin \theta = [E/(E - V_0)] \sin \phi$ and $\cos \theta = \sqrt{1 - \sin^2 \theta}$ are used. The band structure and wavevectors related angles are depicted in Figs. 4(c,g), respectively.

In the regime $0 < V_0 < E$, the refractive index is in the range $1 < n < \infty$ with both the incident and transmitted electron in the conduction band. There is a critical angle in this case determined by $\sin \theta = 1 = [E/(E - V_0)] \sin \phi_c$. The transmission angle can be obtained in the same form as in Eq. (A2). The band structures and wavevectors are illustrated in Figs. 4(d,h), respectively.

Appendix B: Survival probability distribution of α -T₃ quasiparticles in different energy regimes

For completeness, we derive the decay law of the survival probability of α -T₃ quasiparticles and obtain the decay rate in other energy regimes than the Klein tunneling regime. We argue that the decay law in these regimes is practically infeasible for detecting the Berry phase. For example, in the regimes where there is no critical angle, the decay can be too fast for it to be useful. In the regimes where there is a critical angle, the decay for distinct quasiparticles from the material family follows a similar law, making it difficult to distinguish the different quasiparticles.

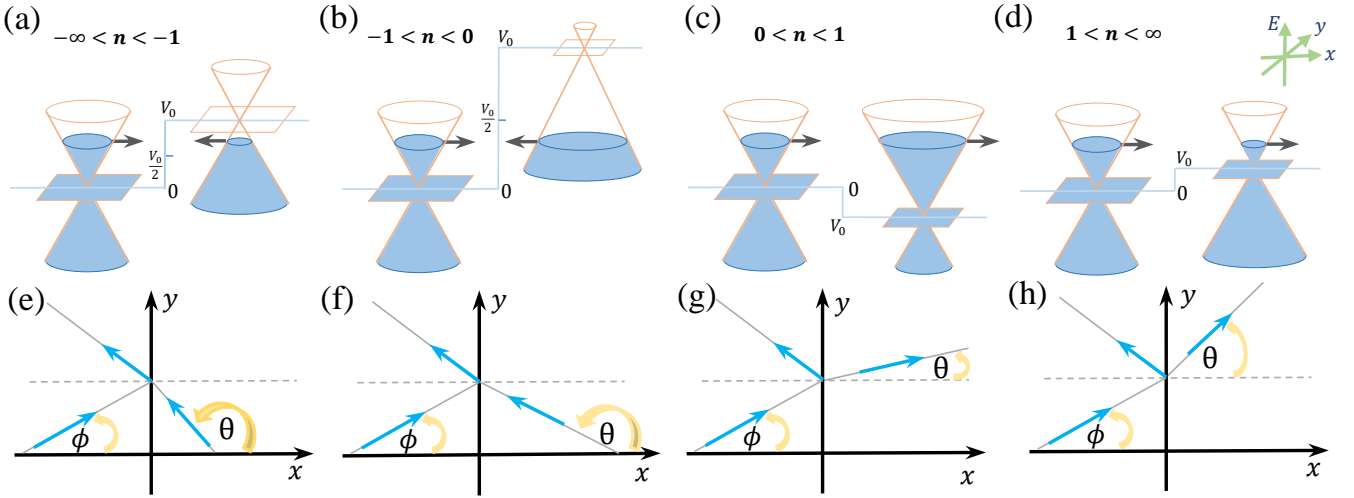


FIG. 4. Schematic illustration of the band structures and wavevectors across a potential step with different values of the refractive index. First row: band structures across the potential step with different values of the gate potential (corresponding to different values of the refractive index) at fixed Fermi energy. The black arrows denote the wavevector directions (only the cases with the wavevector in the x direction are shown). In the regime of negative refractive index, the wavevector directions are reversed. Second row: electron wavevectors with the incident and transmitted angles ϕ and θ , respectively.

1. The $0 < E < V_0/2$ regime

In this energy regime, the refractive index $n = E/(E - V_0)$ of the cavity is in the range $-1 < n < 0$. In this regime, there exists no critical angle for rays inside the cavity. Figure 5(a) shows that the transmission is nonzero for all angles and it increases with decreasing α values. In this case, the decay of quasiparticles is exponential and it does not depend on the nature of the classical dynamics, i.e., integrable or chaotic, as shown in Fig. 5.

A theoretical explanation of the features in Fig. 5 is as follows. Due to the absence of a critical angle for Dirac electron optical rays in the energy range $0 < E < V_0/2$, the survival probability from a circular (integrable) is mainly determined by the ray behavior about $\phi = \pi/2$. Letting $\phi = \pi/2 - x$, where x is a small angle deviation from $\pi/2$, and using the approximations

$$\begin{aligned}\sin \phi &\approx \sin \phi_c - \cos \phi_c \cdot x, \\ \cos \phi &\approx \cos \phi_c + \sin \phi_c \cdot x, \\ \sin \theta &\approx |n| \cdot (\sin \phi_c - \cos \phi_c \cdot x), \\ \cos \theta &\approx -\sqrt{1 - n^2 \cdot (\sin \phi_c - \cos \phi_c \cdot x)^2},\end{aligned}$$

we get

$$\ln R^{-1} = \frac{4x\sqrt{1-n^2}}{2 + 2|n| - \sin^2(2\psi)(1 + |n|)^2}. \quad (\text{B1})$$

where $R = 1 - T$ with T being the transmission coefficient defined in Eq. (2) in the main text. The survival probability can be expressed as

$$P_{sv} = \exp \left\{ -\frac{2\sqrt{1-n^2}}{2 + 2|n| - \sin^2(2\psi)(1 + |n|)^2} \cdot t \right\} \quad (\text{B2})$$

For a chaotic cavity, the angle distribution is random, leading to an exponential behavior of the survival probability. We can obtain the expression for the decay rate γ by approximating P_{sv} as

$$P_{sv}(t) \approx \langle 1 - T(p) \rangle^{t/\langle d \rangle} = \exp \{ \ln [1 - \langle T(p) \rangle] (t/\langle d \rangle) \}. \quad (\text{B3})$$

The decay rate can be expressed as

$$\gamma = -\frac{1}{\langle d \rangle} \ln [1 - \langle T(p) \rangle]. \quad (\text{B4})$$

For either the integrable or the chaotic cavity, the exponential decay rate depends on the material parameter α which, in principle, can be used to detect the Berry phase. However, due to the lack of a critical angle in this energy range, experimentally it would be difficult to confine the quasiparticles. Indeed, comparing with the exponential decay from a chaotic cavity in the Klein tunneling regime ($V_0/2 < E < V_0$) as treated in the main text, here the decay is much faster.

2. The $0 < V_0 < E$ regime

For the energy range $0 < V_0 < E$ with the refractive index $n = E/(E - V_0)$ of the cavity in the range $1 < n < \infty$, the survival probability with time exhibits an algebraic decay from an integrable cavity and an exponential decay from a chaotic cavity, which is characteristically similar to the decay behaviors in the Klein tunneling regime ($V_0/2 < E < V_0$) treated in the main text. A difference is that, for $0 < V_0 < E$, the dependence of the transmission on the material parameter α is much weaker in the sense that, as the value of α is increased

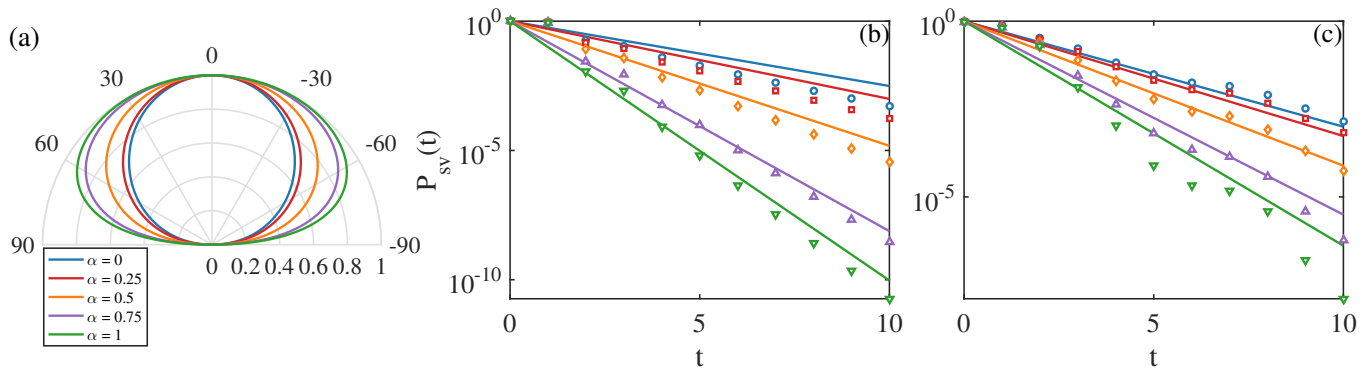


FIG. 5. Survival probabilities from integrable and chaotic cavities for $0 < E < V_0/2$. For $E/V_0 = 1/3$ and $n = -0.5$, (a) transmission versus the incident angle on a polar plot, (b) decay of the survival probability from a circular (integrable) cavity with time, and (c) decay of the survival probability from a stadium shaped (chaotic) cavity.

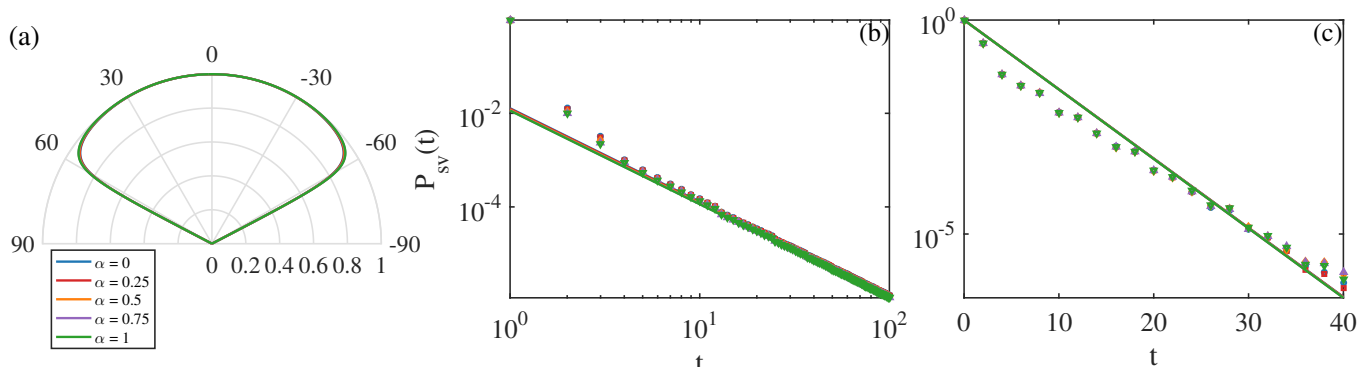


FIG. 6. Survival probabilities from integrable and chaotic cavities for $0 < V_0 < E$. For $E/V_0 = 8.8309$ ($n = 1.1277$), (a) polar representation of the transmission with respect to the incident angle, (b) decay with time of the survival probability from a circular (integrable) cavity, and (c) decay of survival probability from a stadium shaped (chaotic) cavity.

from zero to one, the transmission barely changes. It is thus practically difficult to distinguish the quasiparticles for different materials. These behaviors are shown in Fig. 6, where the analytical fitting is calculated in the same way as in the main text.

3. The $V_0 < 0 < E$ regime

In the energy regime $V_0 < 0 < E$ with the refractive index $n = E/(E - V_0)$ of the cavity in the range $0 < n < 1$, the decay of the survival probability is similar to that in the $0 < E < V_0/2$ regime. In particular, regardless of the nature of the classical dynamics (integrable or chaotic), the survival probability exhibits an exponential decay with time, as shown in Fig. 7. Again, comparing with the energy regime of Klein tunneling, the decay is much faster here, making experimental detection of Berry phase difficult.

Appendix C: Comparison between the decay of survival probability for pseudospin-1/2 and pseudospin-1 quasiparticles

The best studied material in the α -T₃ family is graphene, corresponding to $\alpha = 0$. There is also a growing interest in the material at the other end of the spectrum: $\alpha = 1$ for which the quasiparticles are of the pseudospin-1 nature. We offer a comparison of the decay behavior of the quasiparticles at these two extreme cases.

In the energy range $0 < E < V_0/2$ [corresponding to negative refractive index: $-1 < n = E/(E - V_0) < 0$], there is no critical angle for total internal reflection. For both integrable and chaotic cavities, the survival probability decays exponentially with time, with no qualitative difference. As the absolute value of the refractive index is increased, the range of angle for transmission is large for pseudospin-1 quasiparticles, but the range is smaller for pseudospin-1/2 quasiparticles. For integrable cavities, the difference is somewhat larger.

In the energy range for Klein tunneling: $V_0/2 < E < V_0$ ($-\infty < n < -1$), a critical angle arises, above which there are total internal reflections. For an integrable cavity, the survival probability decays algebraically with

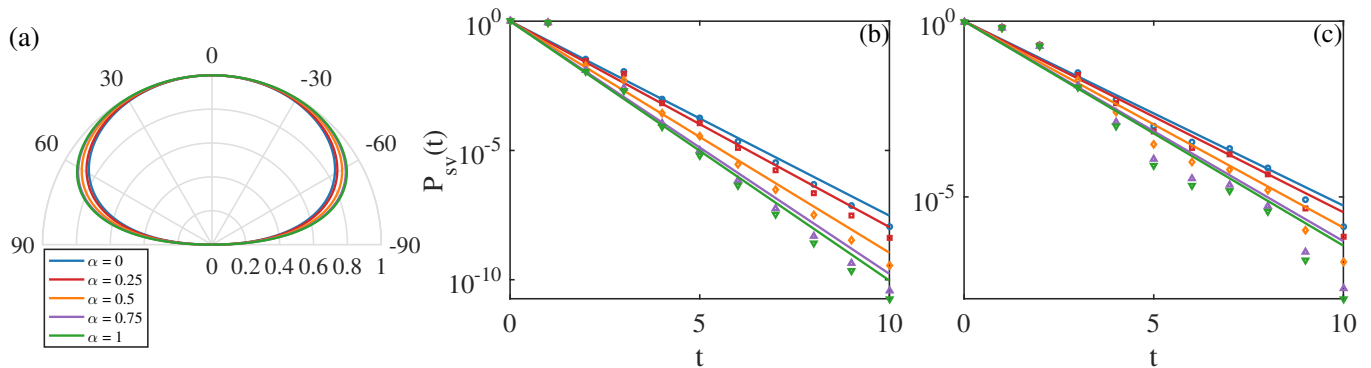


FIG. 7. Survival probability from integrable and chaotic cavities in the $V_0 < 0 < E$ energy regime. For $E/V_0 = -1$ ($n = 0.5$), (a) a polar representation of the transmission versus the incident angle, (b) decay of survival probability from a circular (integrable) cavity, and (c) decay of survival probability from a stadium shaped (chaotic) cavity.

time, but the decay is exponential for a chaotic cavity. In the integrable case, the algebraic decay exponents have approximately identical values for the pseudospin-1 and pseudospin-1/2 particles. However, for a chaotic cavity, the decay of pseudospin-1 quasiparticles is much faster than that of pseudospin-1/2 quasiparticles. Chaos can thus be effective in detecting the Berry phase to distinguish the two types of quasiparticles. In fact, as demonstrated in the main text, chaos in the Klein tunneling regime can be effective for detecting the Berry phase across the entire material spectrum of the α - T_3 family.

In the energy range of $V_0 < E$ ($1 < n < \infty$), a critical angle exists. The decay behavior of the survival probability is algebraic for an integral cavity and exponential for a chaotic cavity. The difference in the transmission versus the incident angle is small for pseudospin-1 and pseudospin-1/2 quasiparticles, leading to a similar value

of the algebraic decay coefficient in the integrable case and a similar exponential decay law in the chaotic case. In this energy range, to use the decay behavior to discern the quasiparticles would be practically difficult.

In the energy range $V_0 < 0 < E$ ($0 < n < 1$), there is no critical angle, and the decay behavior is exponential for both integrable and chaotic cavities. As the energy is increased, the difference in the decay behaviors of pseudospin-1 and pseudospin-1/2 quasiparticles diminishes, ruling out the possibility of exploiting the decay for detection of Berry phase.

Finally, we note a symmetry related phenomenon: for spin-1 quasiparticles the behavior of the survival probability is identical for positive and negative refractive index regimes, as a result of symmetry in the expression of the transmission coefficient.

* Ying-Cheng.Lai@asu.edu

¹ S. Pancharatnam, "Generalized theory of interference, and its applications. part i. coherent pencils," Proc. Indian Acad. Sci. A. **44**, 247 (1956).

² H. C. L. Higgins, U. Öpik, M. H. L. Pryce, and R. A. Sack, "Studies of the jahn-teller effect ii the dynamical problem," Proc. R. Soc. A **244**, 1 (1958).

³ M. V. Berry, "Quantal phase factors accompanying adiabatic changes," Proc. R. Soc. A **392**, 45 (1984).

⁴ Y. B. Zhang, Y. W. Tan, H. L. Stormer, and P. Kim, "Experimental observation of the quantum hall effect and Berry's phase in graphene," Nature **438**, 201 (2005).

⁵ P. Carmier and D. Ullmo, "Berry phase in graphene: Semi-classical perspective," Phys. Rev. B **77**, 245413 (2008).

⁶ G. P. Mikitika and Y. V. Sharlaib, "The berry phase in graphene and graphite multilayers," Low Temp. Phys. **34**, 794 (2008).

⁷ E. Illes, J. Carbotte, and E. Nicol, "Hall quantization and optical conductivity evolution with variable berry phase in the $\alpha - T_3$ model," Phys. Rev. B **92**, 245410 (2015).

⁸ A. K. Geim and K. S. Novoselov, "The rise of graphene,"

Nat. Mater. **6**, 183 (2007).

⁹ A. K. Geim and I. V. Grigorieva, "Van der waals heterostructures," Nature **499**, 419 (2013).

¹⁰ P. Ajayan, P. Kim, and K. Banerjee, "Two-dimensional van der Waals materials," Phys. Today **69**, 38 (2016).

¹¹ L. Duca, T. Li, M. Reitter, I. Bloch, M. Schleier-Smith, and U. Schneider, "An aharonov-bohm interferometer for determining bloch band topology," Science **347**, 288 (2015).

¹² J. F. Rodriguez-Nieva and L. S. Levitov, "Berry phase jumps and giant nonreciprocity in dirac quantum dots," Phys. Rev. B **94**, 235406 (2016).

¹³ F. Ghahari, D. Walkup, C. Gutiérrez, J. F. Rodriguez-Nieva, Y. Zhao, J. Wyrick, F. D. Natterer, W. G. Cullen, K. Watanabe, T. Taniguchi, *et al.*, "An on/off berry phase switch in circular graphene resonators," Science **356**, 845 (2017).

¹⁴ R. Sepkhanov, J. Nilsson, and C. Beenakker, "Proposed method for detection of the pseudospin-1 2 berry phase in a photonic crystal with a dirac spectrum," Phys. Rev. B **78**, 045122 (2008).

¹⁵ B. Sutherland, "Localization of electronic wave functions

- due to local topology,” *Phys. Rev. B* **34**, 5208 (1986).
- 16 D. Bercioux, D. F. Urban, H. Grabert, and W. Häusler, “Massless dirac-weyl fermions in a \sqcup_3 optical lattice,” *Phys. Rev. A* **80**, 063603 (2009).
 - 17 R. Shen, L. B. Shao, B. Wang, and D. Y. Xing, “Single Dirac cone with a flat band touching on line-centered-square optical lattices,” *Phys. Rev. B* **81**, 041410 (2010).
 - 18 D. Green, L. Santos, and C. Chamon, “Isolated flat bands and spin-1 conical bands in two-dimensional lattices,” *Phys. Rev. B* **82**, 075104 (2010).
 - 19 B. Dóra, J. Kailasvuori, and R. Moessner, “Lattice generalization of the Dirac equation to general spin and the role of the flat band,” *Phys. Rev. B* **84**, 195422 (2011).
 - 20 F. Wang and Y. Ran, “Nearly flat band with Chern number $c = 2$ on the dice lattice,” *Phys. Rev. B* **84**, 241103 (2011).
 - 21 X. Huang, Y. Lai, Z. H. Hang, H. Zheng, and C. T. Chan, “Dirac cones induced by accidental degeneracy in photonic crystals and zero-refractive-index materials,” *Nat. Mater.* **10**, 582 EP (2011).
 - 22 J. Mei, Y. Wu, C. T. Chan, and Z.-Q. Zhang, “First-principles study of Dirac and Dirac-like cones in phononic and photonic crystals,” *Phys. Rev. B* **86**, 035141 (2012).
 - 23 P. Moitra, Y. Yang, Z. Anderson, I. I. Kravchenko, D. P. Briggs, and J. Valentine, “Realization of an all-dielectric zero-index optical metamaterial,” *Nat. Photon.* **7**, 791 (2013).
 - 24 D. Guzmán-Silva, C. Mejía-Cortés, M. A. Bandres, M. C. Rechtsman, S. Weimann, S. Nolte, M. Segev, A. Szameit, and R. A. Vicencio, “Experimental observation of bulk and edge transport in photonic Lieb lattices,” *New J. Phys.* **16**, 063061 (2014).
 - 25 J. Romhányi, K. Penc, and R. Ganesh, “Hall effect of triplons in a dimerized quantum magnet,” *Nat. Commun.* **6**, 6805 (2015).
 - 26 G. Giovannetti, M. Capone, J. van den Brink, and C. Ortix, “Kekulé textures, pseudospin-one Dirac cones, and quadratic band crossings in a graphene-hexagonal indium chalcogenide bilayer,” *Phys. Rev. B* **91**, 121417 (2015).
 - 27 Y. Li, S. Kita, P. Muoz, O. Reshef, D. I. Vulis, M. Yin, M. Lonar, and E. Mazur, “On-chip zero-index metamaterials,” *Nat. Photon.* **9**, 738 (2015).
 - 28 S. Mukherjee, A. Spracklen, D. Choudhury, N. Goldman, P. Öhberg, E. Andersson, and R. R. Thomson, “Observation of a localized flat-band state in a photonic Lieb lattice,” *Phys. Rev. Lett.* **114**, 245504 (2015).
 - 29 R. A. Vicencio, C. Cantillano, L. Morales-Inostroza, B. Real, C. Mejía-Cortés, S. Weimann, A. Szameit, and M. I. Molina, “Observation of localized states in Lieb photonic lattices,” *Phys. Rev. Lett.* **114**, 245503 (2015).
 - 30 S. Taie, H. Ozawa, T. Ichinose, T. Nishio, S. Nakajima, and Y. Takahashi, “Coherent driving and freezing of bosonic matter wave in an optical lieb lattice,” *Sci. Adv.* **1**, e1500854 (2015).
 - 31 A. Fang, Z. Q. Zhang, S. G. Louie, and C. T. Chan, “Klein tunneling and supercollimation of pseudospin-1 electromagnetic waves,” *Phys. Rev. B* **93**, 035422 (2016).
 - 32 F. Diebel, D. Leykam, S. Kroesen, C. Denz, and A. S. Desyatnikov, “Conical diffraction and composite Lieb bosons in photonic lattices,” *Phys. Rev. Lett.* **116**, 183902 (2016).
 - 33 L. Zhu, S.-S. Wang, S. Guan, Y. Liu, T. Zhang, G. Chen, and S. A. Yang, “Blue phosphorene oxide: Strain-tunable quantum phase transitions and novel 2d emergent fermions,” *Nano Letters* **16**, 6548 (2016).
 - 34 B. Bradlyn, J. Cano, Z. Wang, M. G. Vergniory, C. Felser, R. J. Cava, and B. A. Bernevig, “Beyond Dirac and Weyl fermions: Unconventional quasiparticles in conventional crystals,” *Science* **353** (2016).
 - 35 I. C. Fulga and A. Stern, “Triple point fermions in a minimal symmorphic model,” *Phys. Rev. B* **95**, 241116 (2017).
 - 36 M. Ezawa, “Triplet fermions and dirac fermions in borophene,” *Phys. Rev. B* **96**, 035425 (2017).
 - 37 C. Zhong, Y. Chen, Z.-M. Yu, Y. Xie, H. Wang, S. A. Yang, and S. Zhang, “Three-dimensional pentagon carbon with a genesis of emergent fermions,” *Nature Communications* **8**, 15641 EP (2017), article.
 - 38 Y.-Q. Zhu, D.-W. Zhang, H. Yan, D.-Y. Xing, and S.-L. Zhu, “Emergent pseudospin-1 maxwell fermions with a threefold degeneracy in optical lattices,” *Phys. Rev. A* **96**, 033634 (2017).
 - 39 R. Drost, T. Ojanen, A. Harju, and P. Liljeroth, “Topological states in engineered atomic lattices,” *Nat. Phys.* **13**, 668 (2017).
 - 40 M. R. Slot, T. S. Gardenier, P. H. Jacobse, G. C. P. van Miert, S. N. Kempkes, S. J. M. Zevenhuizen, C. M. Smith, D. Vanmaekelbergh, and I. Swart, “Experimental realization and characterization of an electronic lieb lattice,” *Nat. Phys.* **13**, 672 (2017).
 - 41 X. Tan, D.-W. Zhang, Q. Liu, G. Xue, H.-F. Yu, Y.-Q. Zhu, H. Yan, S.-L. Zhu, and Y. Yu, “Topological maxwell metal bands in a superconducting qutrit,” *Phys. Rev. Lett.* **120**, 130503 (2018).
 - 42 A. Raoux, M. Morigi, J.-N. Fuchs, F. Piéchon, and G. Montambaux, “From dia-to paramagnetic orbital susceptibility of massless fermions,” *Phys. Rev. Lett.* **112**, 026402 (2014).
 - 43 F. Piéchon, J. Fuchs, A. Raoux, and G. Montambaux, “Tunable orbital susceptibility in $\alpha-T_3$ tight-binding models,” *J. Phys. Conf. Ser.* **603**, 012001 (2015).
 - 44 E. Illes and E. Nicol, “Magnetic properties of the $\alpha - T_3$ model: Magneto-optical conductivity and the hofstadter butterfly,” *Phys. Rev. B* **94**, 125435 (2016).
 - 45 E. Illes and E. Nicol, “Klein tunneling in the $\alpha - T_3$ model,” *Phys. Rev. B* **95**, 235432 (2017).
 - 46 A. D. Kovács, G. Dávid, B. Dóra, and J. Cserti, “Frequency-dependent magneto-optical conductivity in the generalized $\alpha - T_3$ model,” *Phys. Rev. B* **95**, 035414 (2017).
 - 47 J. Cserti, A. Pályi, and C. Péterfalvi, “Caustics due to a negative refractive index in circular graphene p - n junctions,” *Phys. Rev. Lett.* **99**, 246801 (2007).
 - 48 V. V. Cheianov, V. Fal’ko, and B. L. Altshuler, “The focusing of electron flow and a Veselago lens in graphene p - n junctions,” *Science* **315**, 1252 (2007).
 - 49 X. Du, I. Skachko, A. Barker, and E. Y. Andrei, “Approaching ballistic transport in suspended graphene,” *Nat. Nanotech.* **3**, 491 (2008).
 - 50 A. V. Shytov, M. S. Rudner, and L. S. Levitov, “Klein backscattering and Fabry-Pérot interference in graphene heterojunctions,” *Phys. Rev. Lett.* **101**, 156804 (2008).
 - 51 C. W. J. Beenakker, R. A. Sepkhanov, A. R. Akhmerov, and J. Tworzydło, “Quantum Goos-Hänchen effect in graphene,” *Phys. Rev. Lett.* **102**, 146804 (2009).
 - 52 A. G. Moghaddam and M. Zareyan, “Graphene-based electronic spin lenses,” *Phys. Rev. Lett.* **105**, 146803 (2010).
 - 53 N. Gu, M. Rudner, and L. Levitov, “Chirality-assisted electronic cloaking of confined states in bilayer graphene,” *Phys. Rev. Lett.* **107**, 156603 (2011).

- ⁵⁴ J. R. Williams, T. Low, M. S. Lundstrom, and C. M. Marcus, "Gate-controlled guiding of electrons in graphene," *Nat. Nanotech.* **6**, 222 (2011).
- ⁵⁵ P. Rickhaus, R. Maurand, M.-H. Liu, M. Weiss, K. Richter, and C. Schönberger, "Ballistic interferences in suspended graphene," *Nat. Commun.* **4**, 2342 (2013).
- ⁵⁶ B. Liao, M. Zabarjadi, K. Esfarjani, and G. Chen, "Isotropic and energy-selective electron cloaks on graphene," *Phys. Rev. B* **88**, 155432 (2013).
- ⁵⁷ R. L. Heinisch, F. X. Bronold, and H. Fehske, "Mie scattering analog in graphene: Lensing, particle confinement, and depletion of Klein tunneling," *Phys. Rev. B* **87**, 155409 (2013).
- ⁵⁸ M. M. Asmar and S. E. Ulloa, "Rashba spin-orbit interaction and birefringent electron optics in graphene," *Phys. Rev. B* **87**, 075420 (2013).
- ⁵⁹ J.-S. Wu and M. M. Fogler, "Scattering of two-dimensional massless Dirac electrons by a circular potential barrier," *Phys. Rev. B* **90**, 235402 (2014).
- ⁶⁰ Y. Zhao, J. Wyrick, F. D. Natterer, J. F. Rodriguez-Nieva, C. Lewandowski, K. Watanabe, T. Taniguchi, L. S. Levitov, N. B. Zhitenev, and J. A. Strosio, "Creating and probing electron whispering-gallery modes in graphene," *Science* **348**, 672 (2015).
- ⁶¹ P. Rickhaus, M.-H. Liu, P. Makk, R. Maurand, S. Hess, S. Zihlmann, M. Weiss, K. Richter, and C. Schönberger, "Guiding of electrons in a few-mode ballistic graphene channel," *Nano Lett.* **15**, 5819 (2015).
- ⁶² G.-H. Lee, G.-H. Park, and H.-J. Lee, "Observation of negative refraction of Dirac fermions in graphene," *Nat. Phys.* **11**, 925 (2015), letter.
- ⁶³ P. Rickhaus, P. Makk, K. Richter, and C. Schönberger, "Gate tuneable beamsplitter in ballistic graphene," *Appl. Phys. Lett.* **107**, 251901 (2015).
- ⁶⁴ J. D. Walls and D. Hadad, "The talbot effect for two-dimensional massless Dirac fermions," *Sci. Rep.* **6**, 26698 (2016).
- ⁶⁵ J. Caridad, S. Connaughton, C. Ott, H. B. Weber, and V. Krstic, "An electrical analogy to Mie scattering," *Nat. Commun.* **7**, 12894 (2016).
- ⁶⁶ C. Gutiérrez, L. Brown, C.-J. Kim, J. Park, and A. N. Pasupathy, "Klein tunnelling and electron trapping in nanometre-scale graphene quantum dots," *Nat. Phys.* **12**, 1069 (2016).
- ⁶⁷ J. Lee, D. Wong, J. Velasco Jr, J. F. Rodriguez-Nieva, S. Kahn, H.-Z. Tsai, T. Taniguchi, K. Watanabe, A. Zettl, F. Wang, L. S. Levitov, and M. F. Crommie, "Imaging electrostatically confined Dirac fermions in graphene quantum dots," *Nat. Phys.* **12**, 1032 (2016).
- ⁶⁸ S. Chen, Z. Han, M. M. Elahi, K. M. M. Habib, L. Wang, B. Wen, Y. Gao, T. Taniguchi, K. Watanabe, J. Hone, A. W. Ghosh, and C. R. Dean, "Electron optics with p-n junctions in ballistic graphene," *Science* **353**, 1522 (2016).
- ⁶⁹ M. Settnes, S. R. Power, M. Brandbyge, and A.-P. Jauho, "Graphene nanobubbles as valley filters and beam splitters," *Phys. Rev. Lett.* **117**, 276801 (2016).
- ⁷⁰ M.-H. Liu, C. Gorini, and K. Richter, "Creating and steering highly directional electron beams in graphene," *Phys. Rev. Lett.* **118**, 066801 (2017).
- ⁷¹ A. W. Barnard, A. Hughes, A. L. Sharpe, K. Watanabe, T. Taniguchi, and D. Goldhaber-Gordon, "Absorptive pinhole collimators for ballistic Dirac fermions in graphene," *Nat. Commun.* **8**, 15418 (2017).
- ⁷² Y. Jiang, J. Mao, D. Moldovan, M. R. Masir, G. Li, K. Watanabe, T. Taniguchi, F. M. Peeters, and E. Y. Andrei, "Tuning a circular p-n junction in graphene from quantum confinement to optical guiding," *Nat. Nanotech.* **12**, 1045 (2017).
- ⁷³ S.-H. Zhang, J.-J. Zhu, W. Yang, and K. Chang, "Focusing RKKY interaction by graphene p-n junction," *2D Mater.* **4**, 035005 (2017).
- ⁷⁴ P. Båggild, J. M. Caridad, C. Stampfer, G. Calogero, N. R. Papior, and M. Brandbyge, "A two-dimensional Dirac fermion microscope," *Nat. Commun.* **8**, 15783 (2017).
- ⁷⁵ H.-Y. Xu, G.-L. Wang, L. Huang, and Y.-C. Lai, "Chaos in Dirac electron optics: Emergence of a relativistic quantum chimera," *Phys. Rev. Lett.* **120**, 124101 (2018).
- ⁷⁶ J. D. Meiss and E. Ott, "Markov-tree model of intrinsic transport in hamiltonian systems," *Phys. Rev. Lett.* **55**, 2741 (1985).
- ⁷⁷ Y.-C. Lai, M. Ding, C. Grebogi, and R. Blümel, "Algebraic decay and fluctuations of the decay exponent in hamiltonian systems," *Phys. Rev. A* **45**, 4661 (1992).
- ⁷⁸ B. Huckestein, R. Ketzmerick, and C. H. Lewenkopf, "Quantum transport through ballistic cavities: Soft vs hard quantum chaos," *Phys. Rev. Lett.* **84**, 5504 (2000).
- ⁷⁹ M. Weiss, L. Hufnagel, and R. Ketzmerick, "Universal power-law decay in hamiltonian systems?" *Phys. Rev. Lett.* **89**, 239401 (2002).
- ⁸⁰ G. Cristadoro and R. Ketzmerick, "Universality of algebraic decays in hamiltonian systems," *Phys. Rev. Lett.* **100**, 184101 (2008).
- ⁸¹ Y.-C. Lai and T. Tél, *Transient Chaos: Complex Dynamics on Finite-Time Scales* (Springer, New York, 2011).
- ⁸² J. U. Nöckel, A. D. Stone, and R. K. Chang, "Q spoiling and directionality in deformed ring cavities," *Opt. Lett.* **19**, 1693 (1994).
- ⁸³ A. Mekis, J. U. Nöckel, G. Chen, A. D. Stone, and R. K. Chang, "Ray chaos and Q spoiling in lasing droplets," *Phys. Rev. Lett.* **75**, 2682 (1995).
- ⁸⁴ J. U. Nöckel, A. D. Stone, G. Chen, H. L. Grossman, and R. K. Chang, "Directional emission from asymmetric resonant cavities," *Opt. Lett.* **21**, 1609 (1996).
- ⁸⁵ J. U. Nöckel and A. D. Stone, "Ray and wave chaos in asymmetric resonant optical cavities," *Nature* **385**, 45 (1997).
- ⁸⁶ C. Gmachl, F. Capasso, E. E. Narimanov, J. U. Nöckel, A. D. Stone, J. Faist, and D. L. Sivco, "High-power directional emission from microlasers with chaotic resonators," *Science* **280**, 1556 (1998).
- ⁸⁷ E. E. Narimanov, G. Hackenbroich, P. Jacquod, and A. D. Stone, "Semiclassical theory of the emission properties of wave-chaotic resonant cavities," *Phys. Rev. Lett.* **83**, 4991 (1999).
- ⁸⁸ J. Wiersig and M. Hentschel, "Combining directional light output and ultralow loss in deformed microdisks," *Phys. Rev. Lett.* **100**, 033901 (2008).
- ⁸⁹ E. G. Altmann, "Emission from dielectric cavities in terms of invariant sets of the chaotic ray dynamics," *Phys. Rev. A* **79**, 013830 (2009).
- ⁹⁰ X.-F. Jiang, L.-B. Shao, S.-X. Zhang, X. Yi, J. Wiersig, L. Wang, Q.-H. Gong, M. Loncar, L. Yang, and Y.-F. Xiao, "Chaos-assisted broadband momentum transformation in optical microresonators," *Science* **358**, 344 (2017).
- ⁹¹ L. Yang, "Fighting chaos with chaos in lasers," *Science* **361**, 1201 (2018).
- ⁹² S. Bittner, S. Guazzotti, Y.-Q. Zeng, X.-N. Hu, H. Yilmaz, K. Kim, S. S. Oh, Q. J. Wang, O. Hess, and H. Cao,

- “Suppressing spatiotemporal lasing instabilities with wave-chaotic microcavities,” *Science* **361**, 1225 (2018).
- ⁹³ C. Gutiérrez, D. Walkup, F. Ghahari, C. Lewandowski, J. F. Rodriguez-Nieva, K. Watanabe, T. Taniguchi, L. S. Levitov, N. B. Zhitenev, and J. A. Stroscio, “Interaction-driven quantum hall wedding cake-like structures in graphene quantum dots,” *Science* **361**, 789 (2018).
- ⁹⁴ H.-J. Stöckmann, *Quantum Chaos: An Introduction* (Cambridge University Press, 2007).
- ⁹⁵ J.-W. Ryu, S.-Y. Lee, C.-M. Kim, and Y.-J. Park, “Survival probability time distribution in dielectric cavities,” *Phys. Rev. E* **73**, 036207 (2006).
- ⁹⁶ S.-Y. Lee, S. Rim, J.-W. Ryu, T.-Y. Kwon, M. Choi, and C.-M. Kim, “Quasiscattered resonances in a spiral-shaped microcavity,” *Phys. Rev. Lett.* **93**, 164102 (2004).